Available online at www.sciencedirect.com
ScienceDirect
Scripta Materialia 59 (2008) 1135–1138
Scripta MATERIALIA
www.elsevier.com/locate/scriptamat

Creep fracture and load transfer in metal–matrix composite

Ricardo Fernández[1] and Gaspar González-Doncel*

Department of Physical Metallurgy, Centro Nacional de Investigaciones Metalúrgicas (CENIM), CSIC, Av. de Gregorio del Amo 8, E-28040 Madrid, Spain

Received 14 April 2008; revised 3 July 2008; accepted 25 July 2008
Available online 3 August 2008

Creep rupture time data of discontinuously reinforced 6061Al–15 vol.% SiC_w metal–matrix composite (MMC) have been analyzed. Well-known phenomenological models, usually applied to high-temperature structural metals, such as those described by the Monkman–Grant and Larson–Miller equations, have been used. Consistent results are obtained when data are analyzed in the context of the effective stress borne by the metallic matrix. Such analysis supports further the relevance of a load transfer mechanism during creep of these MMCs, as previously suggested.
© 2008 Acta Materialia Inc. Published by Elsevier Ltd. All rights reserved.

Keywords: Metal–matrix composites (MMCs); Aluminum alloys; Powder processing; Creep rupture, High-temperature deformation

In a previous work [1], the creep behavior of a powder metallurgical (PM) 6061Al–15 vol.% SiC_w composite and the corresponding unreinforced 6061Al alloy, also obtained by PM, was investigated. Usually, the creep deformation rate of discontinuously reinforced metal–matrix composites (MMCs) has been explained on the basis of the creep behavior of the matrix alloy and assuming the presence of a threshold stress term, σ_0, such that the following power-law creep relation is satisfied between the steady-state or minimum creep rate, $\dot{\varepsilon}_{min}$, and the applied stress, σ,

$$\dot{\varepsilon}_{min} = A'\left(\frac{\sigma - \sigma_0}{E}\right)^n \exp(-Q_c/RT), \quad (1)$$

where A' is a material's microstructure constant, E is the Young's modulus, n is the stress exponent, Q_c is the activation energy for creep, R is the universal gas constant ($R = 8.314$ kJ mol^{-1} K^{-1}) and T is the absolute temperature. Attempts to understand the significance of σ_0 on the basis of particle-dislocation interaction micromechanisms, however, have failed. On the contrary, it was shown in Ref. [1], that the creep behavior of composites can be understood in terms of the substructure invariant Sherby's model [2] ($n = 8$ in Eq. (1)) and replacing σ_0 by the load carried by the reinforcement, σ_T. In other words, the composite creep rate is dictated by that of the matrix alloy which sustains only part of the applied stress, $(\sigma - \sigma_T)$, due to a partition effect, (under the hypothesis that no damage or deleterious reactions at the metal–ceramic interface occur). In this manner, speculations about the meaning of σ_0 are avoided and a solid new framework of composite creep deformation at high-temperatures can be assumed. The analysis of the experimental results obtained in Ref. [1] was assessed by shear-lag and Eshelby models of the load carried by the reinforcement. In addition, the trends shown from the analysis of data of a number of investigations in the literature on aluminum alloy matrix composites and corresponding unreinforced alloys confirmed the model proposed in Ref. [1].

An important consequence of this new view is that any matrix-dislocation-based plasticity model attempting to account for the creep of the metallic matrix alloy should consider that the actual stress which matrix dislocations bear is $(\sigma - \sigma_T)$. This is contrary to the former view of Eq. (1) (with σ_0 instead of σ_T) in which the stress that the dislocations undergo is directly σ [3].

The purpose of the present research is to validate further this new view of composite creep behavior from creep rupture data obtained from the above PM composite (denoted E219) and the corresponding unreinforced alloy (denoted E220). To this end, available models accounting for phenomenological correlations between time-to-failure and creep data will be used [4–6]. The development of such models, which extrapolate the data obtained from laboratory creep tests, was promoted by the need to know the creep life of engineering structures designed to operate over timescales that can well exceed decades. Typically,

* Corresponding author; e-mail: ggd@cenim.csic.es
[1] Present address: Thin Film R&D Dept. INDO, SA, C/Alcalde Barnils 72, 08174 Sant Cugat del Vallés, Barcelona, Spain.

1359-6462/$ - see front matter © 2008 Acta Materialia Inc. Published by Elsevier Ltd. All rights reserved.
doi:10.1016/j.scriptamat.2008.07.038

laboratory tests are carried out over much shorter time periods, ranging from some few hours up to several months. Obviously, the final objective of these predictions is to prevent catastrophic creep rupture during component service operation. The predictive capacity of these models is, hence, crucial for safe service during the time period for which these structures were designed. One of the key features that guarantees this capacity is that the underlying creep/damage mechanisms which dominate materials deformation should be the same in the short-term creep tests and in the long-term real service condition. Therefore, appropriate data analysis in light of these models may shed further understanding on the creep deformation of structural materials.

It will be shown here that very consistent results between the time-to-rupture data from the above 6061Al–15 vol.% SiC_w PM composite and the corresponding unreinforced alloy are obtained under the assumption that a load partition process is in operation during composite creep deformation.

The materials investigated, the PM processing route and the experimental procedure for the creep tests are described in detail elsewhere [1,7]. Briefly, powder of 6061Al alloy of average particle size less than 45 mm [7] was mixed in a ball–mill with SiC whiskers 20–40 μm in length and average diameter of 0.4 μm [8]. The resulting blend was extruded into a cylindrical bar. The same PM route was used to prepare the 6061Al bulk alloy. Tensile creep tests were carried out under constant stress (4–50 MPa) provided by an Andrade cam and in the temperature range of 573–723 K (300–450 °C). Cylindrical creep specimens 10 mm in gauge length and 3 mm in diameter with threaded heads were machined parallel to the extrusion axis. A load cell, inserted in the loading system, allowed the applied load to be monitored. The sample elongation was measured through linear variable differential transformers suitably attached to the sample. Test data were stored on a computer via appropriate data acquisition boards. Scanning electron microscopy (SEM) was used to investigate the fracture surface of materials.

The results and the analysis of the minimum creep rate dependence with the applied stress were presented in Ref. [1]. It was seen that typical power-law dependence with high stress exponents, in the range of 12.3–27.4, were obtained. The analysis of Ref. [1] demonstrated that the improved creep response of the composite could be explained on the basis of a load transfer mechanism. Here, the time-to-failure data will be analyzed within the same framework.

In Figure 1, the time-to-failure data of the unreinforced alloy (Fig. 1a) and of the composite (Fig. 1b) are plotted as a function of the minimum creep rate on a double logarithmic scale (Monkman–Grant (MG) plots). Some differences between the unreinforced alloy and composite data trends can be appreciated. It can be seen that the data for the unreinforced alloy fit quite well to a common line (Fig. 1a), in agreement with the MG equation [4,5]:

$$t_f \dot{\varepsilon}_{\min}^{n'} = C, \tag{2}$$

where t_f is the time for creep rupture, and n' and C are constants. The constant C is known as the MG constant, and represents the total elongation to failure in case that $n' = 1$ and $\dot{\varepsilon}_{\min}$ dominates during the creep test. $n' = 0.80$

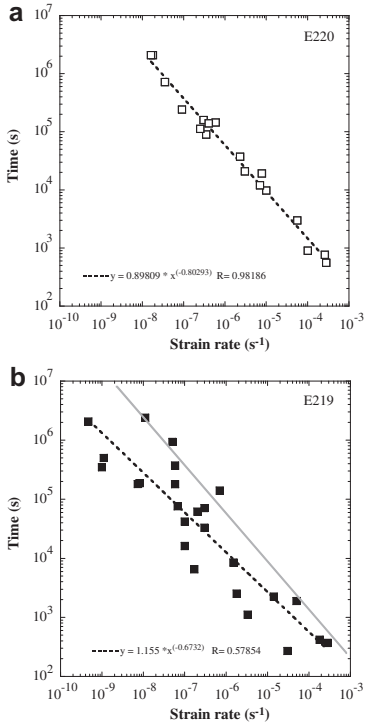

Figure 1. Time to failure as a function of the minimum strain rate for (a) the unreinforced alloy E220 and (b) the composite E219 (Monkman–Grant plots). The data for the unreinforced alloy fit quite well in a common line for any of the testing conditions investigated. The gray solid line in (b) represents, for comparison, the fit obtained for the unreinforced alloy data.

and $C = 0.90$ is obtained. The good common fit obtained ($R^2 = 0.98$) at any of the temperatures and stresses investigated is remarkable.

Several trials to derive the MG equation (with $n' = 1$) from high-temperature fracture mechanisms have been attempted, but none of them can be considered as a conclusive theoretical deduction of the equation from microstructural basis (see e.g. Refs. [9–11]). Although the constant C has a physical meaning (strain) only with an exponent $n' = 1$, the idea underlying this equation (plastic deformation is the macroscopic manifestation of the cumulative damage generated during creep) can be also extended to the majority of cases in which $n' \neq 1$. Despite the empirical nature of the MG relation, Eq. (2), the good fit obtained in Figure 1 reveals common inherent deformation/failure mechanisms in this alloy under any of the testing conditions investigated. The time-to-failure behavior of this alloy in the range of temperatures and applied stresses investigated here is fully predictable from Eq. (2). At this point it is difficult to envisage an explanation from the deviation of the value of n' obtained from the "ideal" $n' = 1$. A deeper analysis of this result is beyond the scope of the present research. It is likely, however, that other processes, such as changes in the microstructure associated with the simultaneous aging process which occurs during testing, are also important for this result.

For the composite (E219 material) the data (Fig. 1b) also obey the MG relation although the fit is more scattered due to the "rougher" microstructure associated with the presence of the reinforcement. The slope ob-

tained is now $n' = 0.67$, which is further from the value of $n' = 1$ than the data of the unreinforced alloy. Again, a full explanation of this value is, at present, speculative. It may be suggested, however, that the deformation and damage mechanism which operate in the unreinforced alloy are also involved in the composite. Of course, additional processes linked to the metal–ceramic interface may be also operative. These phenomena, however, should be not of great relevance as long as previous work [1] suggests that these mechanisms are minimized. On the other hand, it is possible that the difference between the value of n' obtained for the unreinforced alloy and the composite material could arise from the combined action of the load-partitioning phenomenon and the increased pipe diffusion (associated with a larger dislocation density in the composite than in the unreinforced alloy) in the composite material.

It is also seen that the fit for the composite data runs below that for the alloy: for a given value of $\dot{\varepsilon}_{min}$, t_f for the unreinforced alloy is almost two orders of magnitude greater than for the composite, i.e. fracture occurs earlier in the latter material. This is at a first glance a surprising result which accounts for the effect of the reinforcing ceramic particles in the composite: for a given $\dot{\varepsilon}_{min}$ the applied stress in the composite is higher than in the alloy. However, this does not undermine the idea that similar inherent deformation and rupture mechanisms would characterize the alloy and the composite. In agreement with Decker et al. [12], the correlation of creep rupture data with Eq. (2) indicates that creep rupture is controlled by the creep deformation mechanisms.

The trends shown in Figure 1 may therefore suggest that common creep deformation mechanisms are active in both the composite and the alloy and that matrix creep behavior dominates composite deformation at high-temperature. Despite these findings, however, no hint of the load transfer mechanism appears from the plots shown in Figure 1. This is because the applied stress is not a variable to be considered in predictions from the MG relation.

Another phenomenological model for material creep life prediction, probably the most widely used in engineering, is that described by the Larson–Miller parameter, P_{LM} [6]. This model relates P_{LM} with σ, T and t_f, assuming that Eq. (2) is obeyed. The model operates, hence, considering the applied stress as an independent factor. The Larson–Miller parameter model is derived from the Arrhenius dependence of the minimum creep rate and considering that Eq. (2) is obeyed. Accordingly, the following equation is obtained [6]:

$$P_{LM} = T(\log(t_f + K)), \tag{3}$$

where K is a constant obtained from the experimental data and is equal to $K = 46$. For simplicity, the same K value for both the unreinforced alloy and the composite has been assumed given the reasonable similar microstructures and creep deformation mechanisms of both materials [1].

The Larson–Miller parameter varies with stress such that at a given stress level, there are different combinations of T and t_f which lead to the same P_{LM} for a given stress.

As was shown in Figure 4 of Ref. [1], the power-law dependence is obeyed for both the unreinforced alloy and the composite. Considering also the fits shown in Figure 1, it is expected that reasonable Larson–Miller plots can be obtained for these materials. This is confirmed by the trends shown in the plot of Figure 2a. In this figure, the Larson–Miller plot of σ as a function of P_{LM} is shown for the unreinforced alloy and the composite data obtained in this investigation. It is seen that distinguishable behaviors for each material are obtained. Both trends run nearly parallel but separate from each other. As suggested above from a previous study by the present authors [1], however, an appropriate analysis of composite creep data should consider the role of the load transfer mechanisms from matrix to the reinforcement, i.e. that the actual stress carried by the plastically deforming phase of the composite, the metallic matrix, is $(\sigma - \sigma_T)$ instead of the applied stress, σ. In Ref. [1] an appropriate separation of the matrix strengthening due to a finer matrix composite microstructure and load transfer strengthening was used. This allowed calculation of the precise effective stress carried by the composite matrix (and in turn, the load carried by the reinforcement). The data under the different conditions, as calculated in Ref. [1] by comparing the creep behavior of the composite and the unreinforced alloy, are summarized in Table 1. Consequently, a plot similar to that shown in Figure 2a but considering the effective stress, $(\sigma - \sigma_T)$, instead of σ, can be now constructed. As a result from this analysis, the tendency shown in the plot of Figure 2b is obtained. Here, the same data obtained to represent the plot of Figure 2a have been replotted,

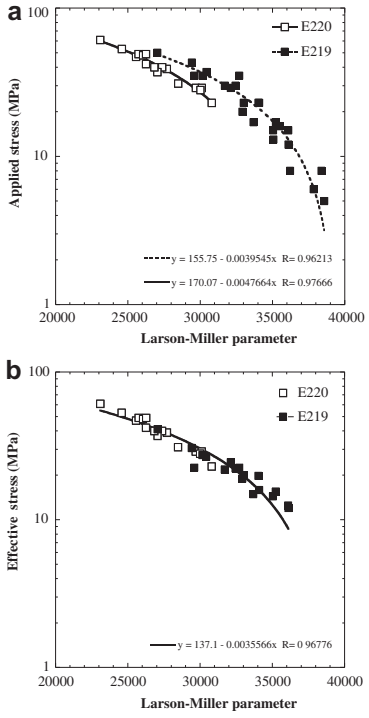

Figure 2. Larson–Miller plot for the unreinforced alloy and the composite data. (a) The applied stress vs. the Larson–Miller parameter for both materials. (b) The effective stress $(\sigma - \sigma_T)$ on the aluminium matrix alloy of the composite (and the applied stress for the unreinforced alloy) vs. the Larson–Miller parameter. By definition, the value of P_{LM}, varies with the stress through the empirical constant K. The good correlation between data for the unreinforced alloy and the composite, assuming effective stress in the latter case, is remarkable.

Table 1. Creep conditions and fracture data for the PM Al6061 alloy (E220) and Al6061–15 vol.% SiC_w composite material (E219)

Temperature (K)	Applied stress (MPa)	Time to fracture (s)
523	40	7.2E + 05
523	48	1.6E + 05
523	49	9.0E + 04
523	49	2.4E + 05
523	53	9.8E + 03
523	61	5.6E + 02
573	28	2.1E + 06
573	31	1.5E + 05
573	37	1.2E + 04
573	40	2.1E + 04
573	42	3.0E + 03
573	47	9.0E + 02
623	23	1.1E + 05
623	29	1.9E + 04
623	29	3.8E + 04
623	39	7.7E + 02

Temperature (K)	Applied stress (MPa)	Effective stress (MPa)	Time to fracture (s)
623	35	23	2.4E + 06
623	35	23	1.6E + 04
623	29	25	9.3E + 05
623	37	27	6.2E + 04
623	50	41	2.7E + 02
673	17	16	3.7E + 05
673	23	16	2.1E + 06
673	23	20	3.5E + 05
673	23	20	7.6E + 04
673	30	22	3.3E + 04
673	35	27	1.1E + 03
673	43	31	3.7E + 02
723	12	12	1.8E + 05
723	15	13	1.9E + 05
723	15	14	4.2E + 02
723	17	15	6.5E + 03
723	20	19	2.3E + 03
723	30	22	4.2E + 02
773	5.0	5.0*	1.8E + 05
773	6.0	6.0*	7.1E + 04
773	8.0	8.0*	8.5E + 03
773	13.0	13.0*	1.9E + 03

but considering that it is the effective stress, $(\sigma - \sigma_T)$, i.e. the one that the composite matrix undergoes during creep deformation. As can be seen here, and contrary to what is appreciated in Figure 2a, both the unreinforced alloy and the composite follow a remarkably common behavior and hence account for (i) the relevant role played by the load transfer mechanisms during creep and fracture deformation and (ii) the common inherent deformation/fracture mechanisms in both the unreinforced alloy and the composite of this investigation. Despite the fact that the fit in Figure 2b diverges somewhat with respect to that for the unreinforced alloy in Figure 2a, the good agreement of all the data is remarkable.

Finally, a comparison of the fracture surface of the unreinforced alloy and the composite is shown from the SEM pictures of Figure 3. The micrograph of Figure 3a is of the unreinforced alloy and Figure 3b is of the composite. The surfaces correspond to samples in which fracture occurred under similar testing conditions. As can be seen, a typical ductile fracture, with the presence of dimples associated with local plastic deformation in the interior of the grains and, hence, with a transgranular type of fracture, is apparent. The composite also shows the presence of the reinforcing particles around which the plastically deformed regions are formed. In essence, these micrographs also suggest that similar deformation/fracture mechanisms are underlying in the creep process of these materials.

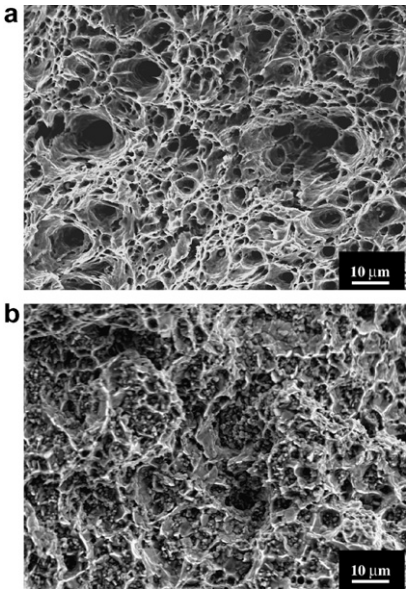

Figure 3. Fracture surfaces of (a) the unreinforced alloy and (b) the composite tested at 623 K and applied stress indicated. For the case of the composite the effective stress on the matrix alloy calculated was 34 MPa (applied stress 42 MPa). A surface of similar aspect with dimples associated with a transgranular and ductile fracture is evident in both micrographs. (a) Al6061; 623 K, 39 MPa; (b) Al6061+15vol.% SiC_w; 623 K, 42 MPa.

In summary, it has been shown that time-to-failure data of aluminum alloy MMC, as analyzed assuming a load transfer mechanism and comparing data with that of the corresponding unreinforced alloy, leads to consistent results which validate further the relevant role of load partition during composite creep deformation.

Financial support from MEC (Ministerio de Educación y Ciencia), Spain, under project MAT05-00527 is acknowledged.

[1] R. Fernández, G. González-Doncel, Acta Mater. 56 (2008) 2549.
[2] O.D. Sherby, R.H. Klundt, A.K. Miller, Metall Trans. 8A (1977) 843.
[3] K.-T. Park, E.J. Lavernia, F.A. Mohamed, Acta Metall. Mater. 38 (1990) 2149.
[4] F.C. Monkman, N.J. Grant, Proc. ASTM 56 (1956) 593.
[5] D.C. Dunand, B.Q. Han, A.M. Jansen, Metall. Mater. Trans. A30 (1999) 829.
[6] F.R. Larson, J. Miller, Am. Soc. Mech. Eng. 74 (1952) 756.
[7] R. Fernández, G. González-Doncel, J. Alloys Compd. 440 (2007) 158.
[8] A. Borrego, J. Ibáñez, V. López, M. Lieblich, G. González-Doncel, Scr. Mater. 34 (1996) 471.
[9] G.H. Edwards, M.F. Ashby, Acta Metall. 27 (1979) 1505.
[10] A. Needleman, J.C. Rice, Acta Metall. 28 (1980) 1315.
[11] A.C.F. Kocks, M.F. Ashby, Prog. Mater. Sci. 27 (1982) 189.
[12] M.W. Decker, J.R. Groza, J.C. Gibeling, Mater. Sci. Eng. A369 (2004) 101.